Electronic Supplementary Material (ESI) for Materials Chemistry Frontiers.

Electronic Supplementary Information (ESI)

Layered double hydroxides as advanced track to promote ionic conductivity in metal borohydride

Yibo Dou, Heine Anton Hansen, Si-Min Xu, and Didier Blanchard*

Dr. Y. Dou, Dr. H. A. Hansen, Dr. D. Blanchard, Department of Energy Conversion and Storage, Technical University of Denmark, Kgs. Lyngby. 2800, Denmark

E-mail : dibl@dtu.dk

Dr. S.-M. Xu, State Key Laboratory of Chemical Resource Engineering, Beijing University of Chemical Technology, Beijing, 100124, P. R. China

1. Experimental section

1.1 Structural characterization

Structural characterization was performed, scanning electron microscopy (SEM) and X-ray diffraction (XRD), X-ray photoelectron spectroscopy (XPS) measurements in airtight sample holders. We recorded the signals five times at the same location for MgAl-LDH/LiBH4 and LiBH4. No obvious variation for Li and B XPS signals were observed during the cycle measurement. The result demonstrated the stability of MgAl-LDH/$LiBH_4$ and $LiBH_4$ during the measurement. SEM images were acquired with a SEM (Zeiss Merlin) with a low acceleration voltage of 10 kV to avoid $LiBH_4$ decomposition and combined with energy-dispersive X-ray spectroscopy (EDX) for the determination of composition. In addition, a fast-recording time, 3 μs pixel-dwell time, was used to limit the beam damage. SEM images were acquired with a SEM (Zeiss Merlin) with an accelerating voltage of 15 kV, combined with energy-dispersive X-ray spectroscopy (EDX) for the determination of composition. A small amount of sample was placed on a SEM plateholder in the glovebox and transferred into the microscope. The samples are exposed to air for no longer than 15 s. Energy-dispersive X-ray spectroscopy (EDX) were used for elemental analysis. XRD patterns are obtained at RT, varying 2θ from 5 to 60°, with a Bruker-D8 Advance X-ray diffractometer setup using Cu Kα 1,2 radiation with λ = 1.5406 Å. The Differential Scanning Calorimetry (DSC) measurements were performed with an apparatus from NETZSCH (Type 200 F3). The samples were measured while ramping at 5 K/min under a nitrogen flow of 20 mL/min. XPS measurement was performed in an ESCALAB 250 instrument (Thermo Electron) with Al Kα radiation.

1.2 Mass Spectrometry.

Mass spectrometry measurements were performed using a OMNISTAR GSD spectrometer. Gas samples were taken from the milling vials and injected into the mass spectrometer column using a syringe. First pure argon was injected, to give the background signal, then the samples from the vial and

then Ar again. The m/z currents for Ar and H_2, i.e. m/z = 40 and 2 were recorded.

1.3 Transport and transference number measurements (MgAl-LDH/$LiBH_4$ (3:7)).

The transference number corresponding to the ionic (t_{ion}) transport has been determined for the MgAl-LDH/$LiBH_4$ SSE using the DC voltage polarization technique.[1] A voltage of 0.5 V was applied across the SSE, using stainless steel blocking electrodes on both sides, and the resulting current was monitored as a function of time (Fig. S13). The mean value of the measured current during 6 hours is 5.45×10^{-6} μA cm^{-2} and results from the instrumental noise. The ionic transport number (t_{ion}) was evaluated using the equation, $t_{ion} = (i_{ion})/i_T$, where i_T, the initial current consists of the sum of the ionic (i_{ion}) and electronic (i_e) currents giving $i_{ion} = i_T - i_e$, and i_e is the final electronic current. The calculated value in this case is found to be $t_{ion} \approx 1$, indicating that the current through the electrolyte is ionic, as there is no remaining current after the initial charging of the system. The lithium transport number (t_+) was estimated by following the procedure of Bruce, Evans and Vincent. [2-4] The solid electrolyte is sandwiched between two cation reversible electrodes (in this case Li metal) and is polarized by the application of a small constant potential difference between the electrodes (ΔV = 10 mV). Under the electric field, positive and negative ions can migrate to the oppositely polarized electrode. The anion concentration is depleted at the negatively polarized electrode and anions accumulate near the positively polarized electrode. Since the number of charge carriers (anions and cations) remains constant, electro-neutrality within the electrolyte must be maintained and a concentration gradient is established. As a consequence, the value of the initial current (I^0) decreases with time until a steady-state current (I^s), due to the sole migration of cations, is eventually observed (Fig. S14). In ideal cases, a direct measure of I^s and I^0 is sufficient to calculate transport numbers (i.e. $t_+ = I^s/I^0$), but in practical cells with active electrodes, the influence of the electrode processes has to be taken into account and, more specifically, the possible changes of resistivity at the electrolyte-electrode interface with polarization. Therefore, EIS measurements were performed to evaluate the resistivity of the cell prior to (R^0) and after (R^s) the polarization procedure, in order to correct for changes in the electrode-electrolyte interface (Fig. S14). For the MgAl-LDH/$LiBH_4$ (3:7) SSE, the transport number of cation (t_+) has been evaluated to be 0.98 using the following equation:

$$t^+ = \frac{I^s}{I^0} \cdot \frac{\Delta V - I^0 R^0}{\Delta V - I^s R^s}$$

and the measured values of I^s, I^0 and R^s, R^0 (Fig. S14 and S15). Therefore, we conclude that the transport of charges is mainly due to the migration of the cations.

2 Theoretical simulation

2.1 DFT for composition determination

DFT calculations of oxyhydroxide formation energy and band gaps were performed using the Atomic Simulation Environment[5] and the GPAW DFT code.[6,7] One-electron wave functions are expanded in plane waves with kinetic energies below 500 eV. Periodically repeated oxyhydroxide units are separated by 13 Å of vacuum. Atom positions are optimized until the largest cartesian force component is below 0.04 eV/Å. 2D oxyhydroxide sheets are modeled using a hexagonal 2 x 2 surface unit cell. Optimizations of 2D oxyhydroxide sheets are performed using a 6 x 6 x 1 grid Monkhorst-Pack grid of k-points, whereas band gaps are calculated on a denser 12 x 12 x 1 Monkhorst-Pack grid of k-points.[8] 1D oxyhydroxide wires are modeled using a 2 x 4 surface cell and a 6 x 1 x 1 Monkhorst-Pack grid of k-points for geometry optimization, while the band gap is calculated on a 12 x 1 x 1 grid. See also Fig. S1.

The revised Perdew-Burke-Ernzerhof (RPBE) exchange correlation functional is used with a Hubbard U correction applied to 3d transition metal valence electrons to provide an improved description of the electronic structure including the band gap.[9,10] Effective U-J values are applied to match the experimental reaction enthalpy of the reaction[11]

$$XO + H_2O \rightarrow XOOH + ½\ H_2.$$ Equ. S1.

The stability of X doped AlOOH sheets is assessed from the reaction:

$$AlOOH + XOOH_{1+x} \rightarrow XAl_3O_4H_{4+x}$$ Equ. S2.

Where AlOOH the aluminum oxyhydroxide sheet, and $XOOH_{1+x}$ a reference (oxy)-hydroxide sheet of the metal X, and $XAl_3O_4H_{4+x}$ is the X doped AlOOH sheet (Table S1).

The stability of doped AlOOH nanowires is assessed from the reaction:

$$Al_8O_{16}H_8 + XOOH_{1+x} \rightarrow XAl_7O_{16}H_{8+x} + AlOOH$$ Equ. S3.

Here, $Al_8O_{16}H_8$ is an aluminum oxyhydroxide wire and $XAl_7O_{16}H_{8+x}$ the X doped aluminum oxyhydroxide wire.

Table S1. Calculated stability of dopants at or near edges of 1D nano wires and in 2D sheets. (ΔE in eV)

	edge	near edge	bulk
Co(II)	-0.09	0.36	0.54
Co(III)	-0.76	-0.05	0.03
Ca(II)	-0.12	0.05	1.52
Zn(II)	-0.82	-0.20	0.18
Mg(II)	-0.62	-0.23	0.60
Ni(II)	-0.66	0.34	0.57
Cr(III)	0.19	0.12	0.11
Mn(III)	-0.77	0.05	0.27
Y(III)	0.61	0.58	0.33
Sc(III)	0.18	0.32	0.49

2.2 DFT for ionic mobility evaluation

Model Construction: The model of bulk MgAl-LDH was built with the space group of $P\bar{3}m1$, with the lattice parameters of $a = b = 3.08$ Å, $c = 7.86$ Å, $\alpha = \beta = 90°$, $\gamma = 120°$.[12] The supercell of bulk MgAl-LDH was 3 × 3 × 1 in the *a*-, *b*-, and *c*- directions. The molar ratio of Mg to Al was 2: 1. Carbonate anion was intercalated into the interlayer gallery of MgAl-LDH. After that, the (003) facet of MgAl-LDH was cleaved containing one bilayer of atoms and vacuum layer of 15 Å. The model of $LiBH_4$ was constructed according to the experimental X-ray diffraction measurement.[13] The space group of $LiBH_4$ was pnma, with the lattice parameters of $a = 7.141$ Å, $b = 4.431$ Å, $c = 6.748$ Å, $\alpha = \beta = \gamma = 90°$. The supercell of $LiBH_4$ was 1 × 2 × 2 in the *a*-, *b*-, and *c*- directions. Thus, the chemical formula of $LiBH_4$ was $Li_{16}B_{16}H_{64}$. The model of MgAl-LDH&$LiBH_4$ was built by integrating the (003) facet of MgAl-LDH and the (001) facet of $LiBH_4$ in one cell with the lattice parameters of $a = 15.692$ Å,

b = 9.060 Å, c = 14.535 Å, $\alpha = \beta = \gamma = 90^{o}$. Four H defects were introduced in MgAl-LDH. Therefore, the chemical formula of $Mg_{12}Al_6O_{54}H_{32}C_6Li_{16}B_{16}H_{60}$.

Computational Methods: All the DFT calculations of ionic mobility were performed with the CASTEP code in the Materials Studio 6.1 software package (Accelrys Software Inc., San Diego, CA).[14] The DFT calculations were performed using a plane wave implementation[15] with the generalized gradient approximation (GGA) Perdew-Burke-Ernzerhof (PBE) as the exchange-correlation functional.[16] The ionic cores were described by the ultrasoft pseudopotentials to improve transferability and reduce the number of plane waves needed in the expansion of the Kohn-Sham orbitals.[17,18] The potential energy surface was searched with the Broyden-Fletcher-Goldfarb-Shanno (BFGS) algorithm.[19] The cut-off energy was set as 380 eV. The geometry optimization was based on three points: (1) the energy tolerance of 1.0×10^{-5} eV per atom, (2) the force tolerance of 0.03 eV/Å, and (3) the displacement tolerance of 1.0×10^{-3} Å. The formula of the reaction between MgAl-LDH and $LiBH_4$ was:

$$MgAl\text{-}LDH + LiBH_4 \rightarrow MgAl\text{-}LDH/LiBH_4 + H_2 \qquad \text{Equ. S4.}$$

The Gibbs free energies of reactant and product were obtained by analyzing their phonon density of states. In *ab initio* molecular dynamics (AIMD) simulations, the time step of 1 fs and time length of 20 ps were applied. The temperature was set as 298.15 K and a Nose thermostat was employed for the canonical ensemble (NVT) AIMD simulations.

3 Additional Figures and Tables.

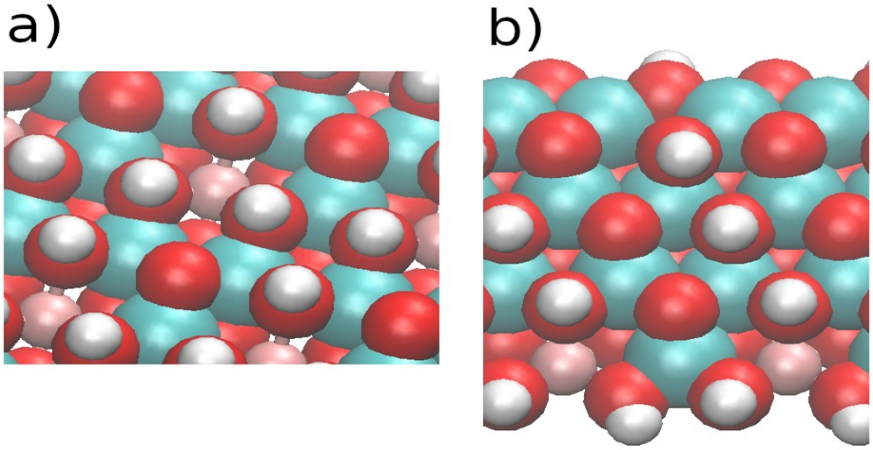

Fig. S1. (a) Top view of $MAl_7O_{16}H_{8+x}$ 2D sheet. (b) Al-LDH 1D nanowire doped at the edge. H is white, O is red, Al is cyan, M dopant is pink.

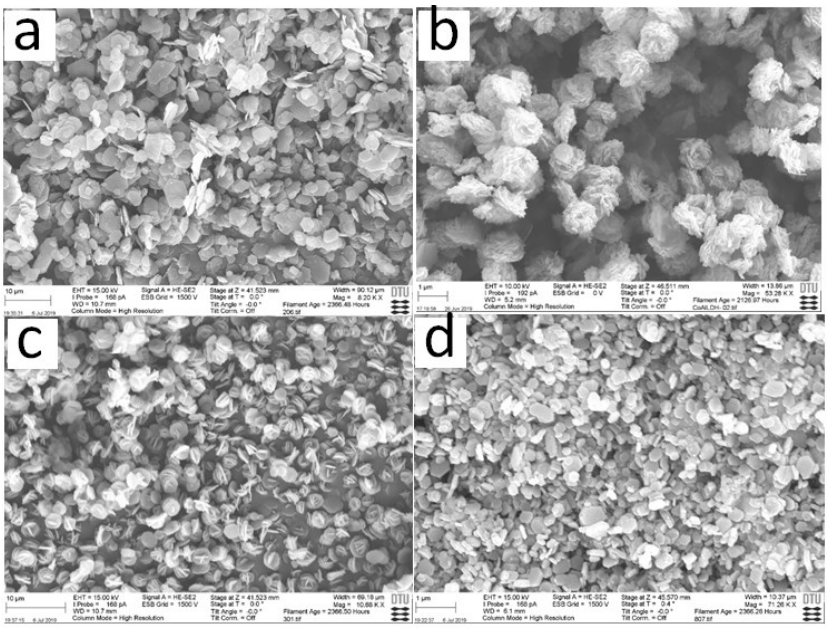

Fig. S2. The SEM images of prepared (a) MgAl-LDH, (b) ZnAl-LDH, (c) CoAl-LDH, and (d) CaAl-LDH, respectively.

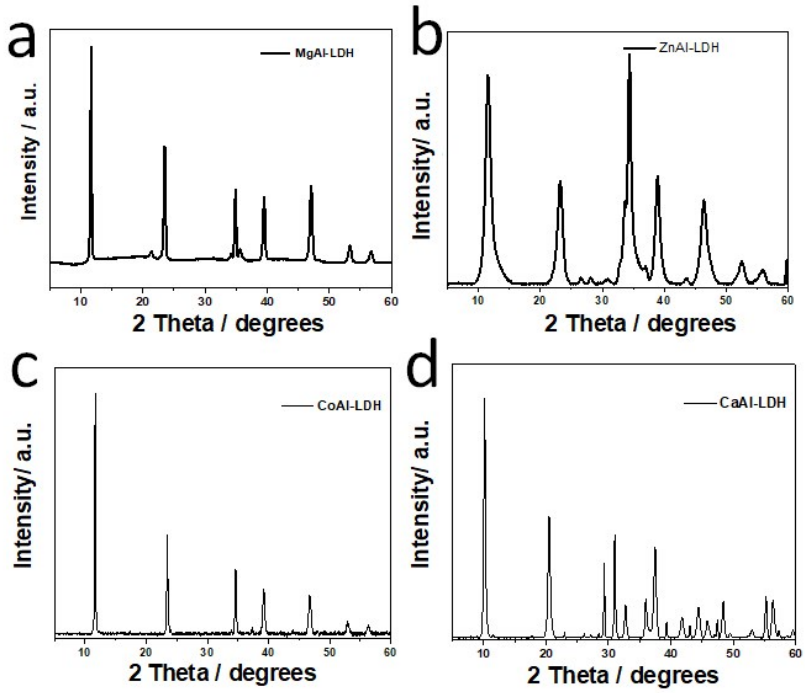

Fig. S3. The XRD patterns of prepared (a) MgAl-LDH, (b) ZnAl-LDH, (c) CoAl-LDH, and (d) CaAl-LDH, respectively.

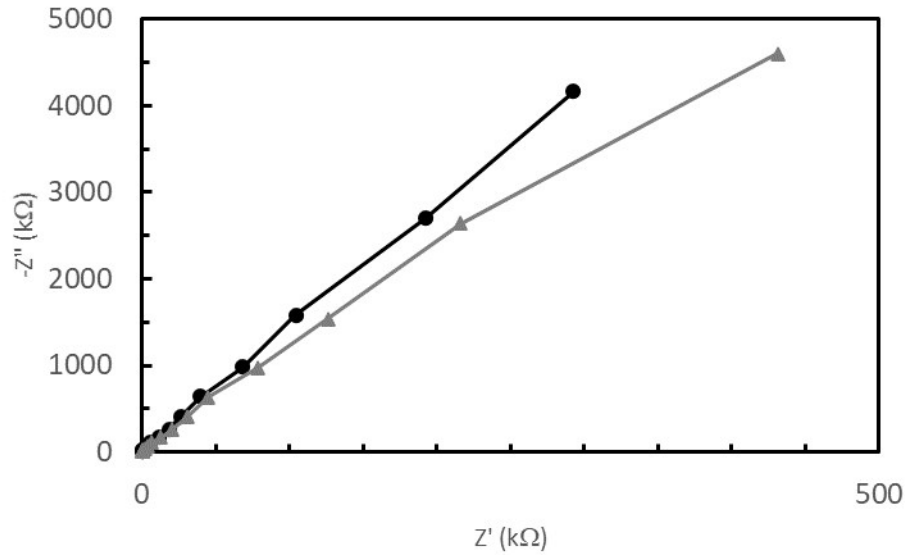

Fig. S4. Electrochemical Impedance Spectroscopy measurements on MgAl-LDH. The results show no electronic nor ionic conductivity. The impedance spectra were recorded for two temperatures (30 and 100 ^{o}C), black and gray symbols respectively, and gave straight lines with intercepts at zero, typical of blocking electrode measurement. No current, ionic or electronic was detected. MgAl-LDH can therefore be considered as an electronic /ionic insulator.

Table S2. The summary of prepared XAl-LDH/M-BH_4 SSEs with various ratio.

SSEs	Weight ratio of LDH: M-BH_4	SSEs	Weight ratio of LDH: M-BH_4
ZnAl-LDH/$LiBH_4$	7:3	MgAl-LDH/$NaBH_4$	3:7
CoAl-LDH/$LiBH_4$	7:3	MgAl-LDH/$NaBH_4$	1:9
CaAl-LDH/$LiBH_4$	7:3	MgAl-LDH/$Mg(BH_4)_2$	7:3
MgAl-LDH/$LiBH_4$	7:3	MgAl-LDH/$Mg(BH_4)_2$	5:5
MgAl-LDH/$LiBH_4$	5:5	MgAl-LDH/$Mg(BH_4)_2$	3:7
MgAl-LDH/$LiBH_4$	3:7	MgAl-LDH/$Mg(BH_4)_2$	1:9
MgAl-LDH/$LiBH_4$	1:9	CoAl-LDH/$Mg(BH_4)_2$	3:7
MgAl-LDH/$NaBH_4$	7:3	CaAl-LDH/$Mg(BH_4)_2$	3:7
MgAl-LDH/$NaBH_4$	5:5	ZnAl-LDH/$Mg(BH_4)_2$	3:7

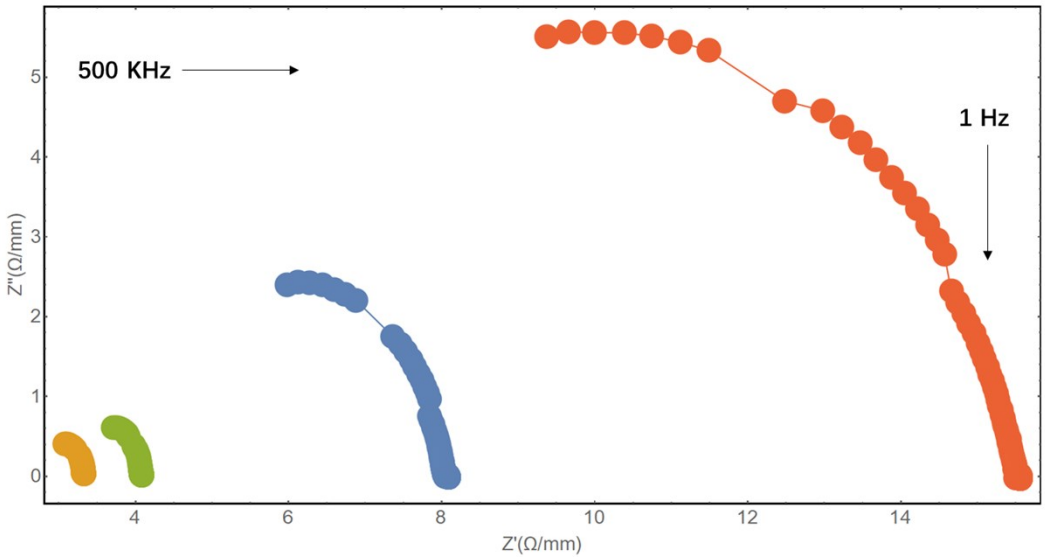

Fig. S5. Examples of the Nyquist plots for MgAl-LDH/$LiBH_4$ with different weight ration and at 40°C. Yellow: 3:7 at 38 °C, blue: 1:9, green: 5:5 and orange: 7:3. Due to the high conductivity of the SSEs and the limitation in the high frequency range, the full semicircle could not be recorded (from 500 kHz to 1 Hz). Some frequency points were removed from the spectra because appearing with systematic noise due to the instrument.

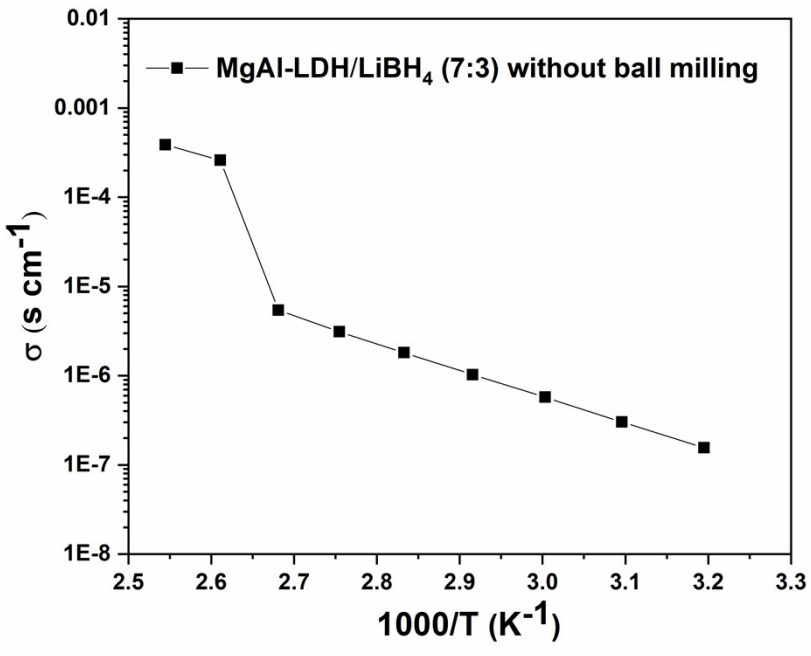

Fig. S6. Arrhenius plots of the ionic conductivities as function of temperature for MgAl-LDH/$LiBH_4$ with weight ratio of 7:3 and without ball milling.

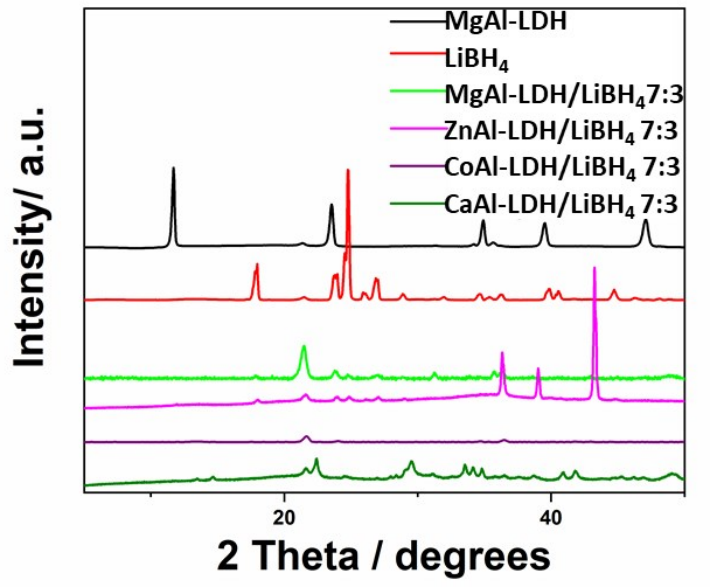

Fig. S7. The XRD patterns of prepared pristine MgAl-LDH, pristine $LiBH_4$, various XAl-LDH/$LiBH_4$ with ratio of 7:3, respectively.

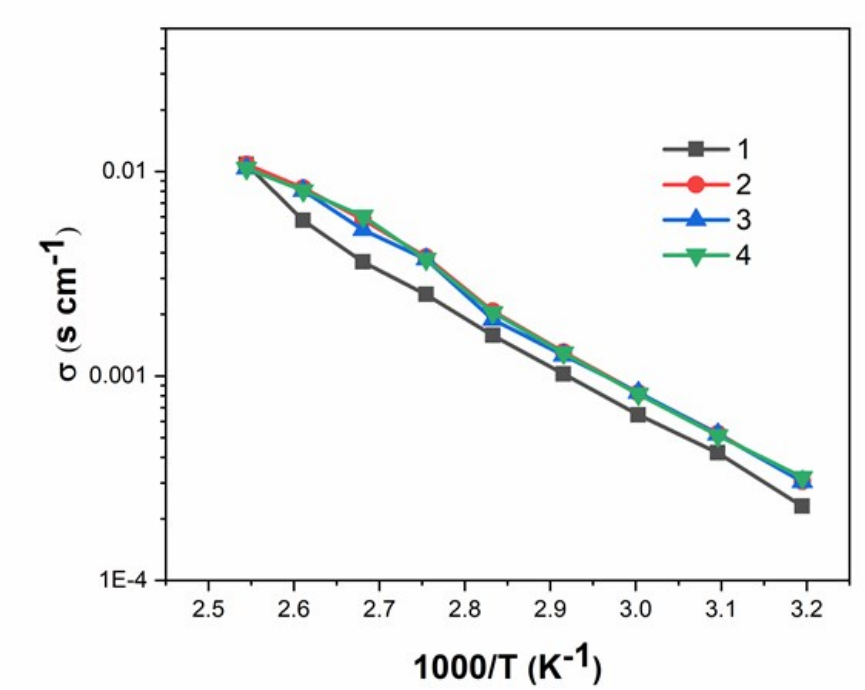

Fig. S8. The stability test of the MgAl-LDH/$LiBH_4$ (3:7) by performing multiple cycles in temperature between 30 and 120 ^oC.

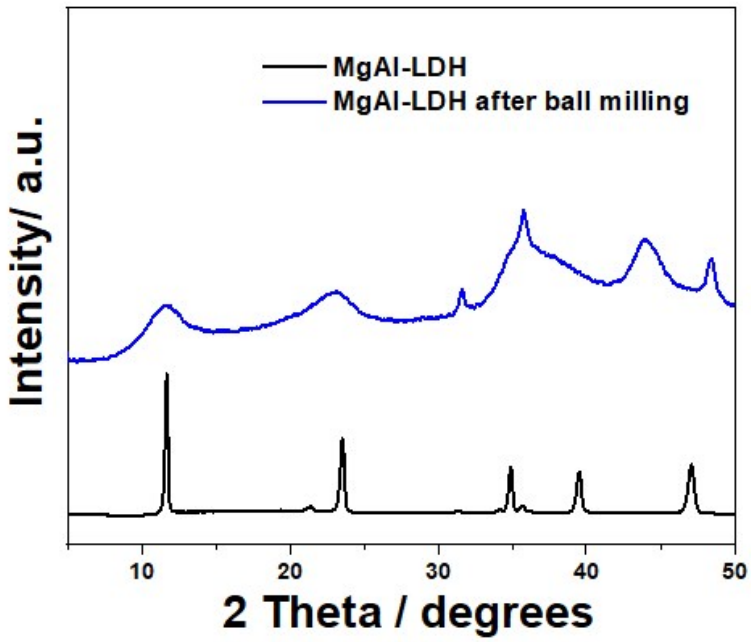

Fig. S9. The XRD patterns of prepared pristine MgAl-LDH before and after ball milling.

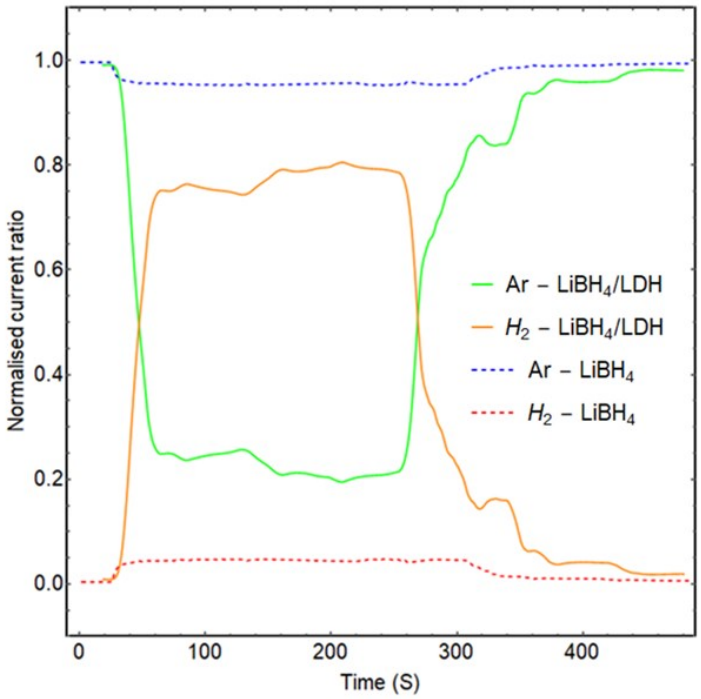

Fig. S10. Normalized current obtained from mass spectrometry gas analysis on the gases contained in the milling vials after milling under the same condition $LiBH_4$ and MgAl-LDH/$LiBH_4$ (3:7). Note that while for $LiBH_4$ at small amount of hydrogen is released, about 55 times more is released for MgAl-LDH/$LiBH_4$ (3:7). See Fig. S11.

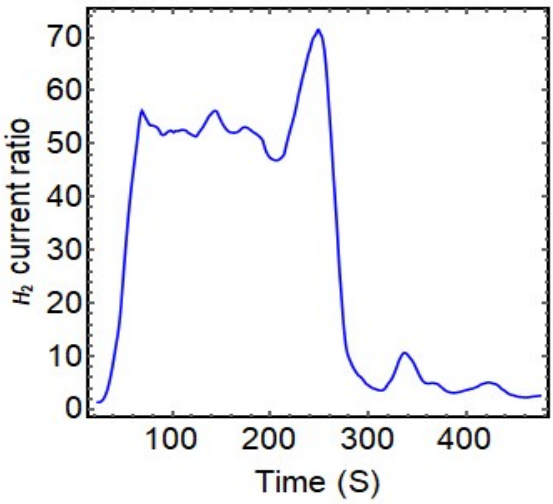

Fig. S11. Ratio of the values of the current obtained for H_2 (m/z = 2) for the gases contained in the milling vials after milling under the same condition $LiBH_4$ and MgAl-LDH/$LiBH_4$ (3:7).

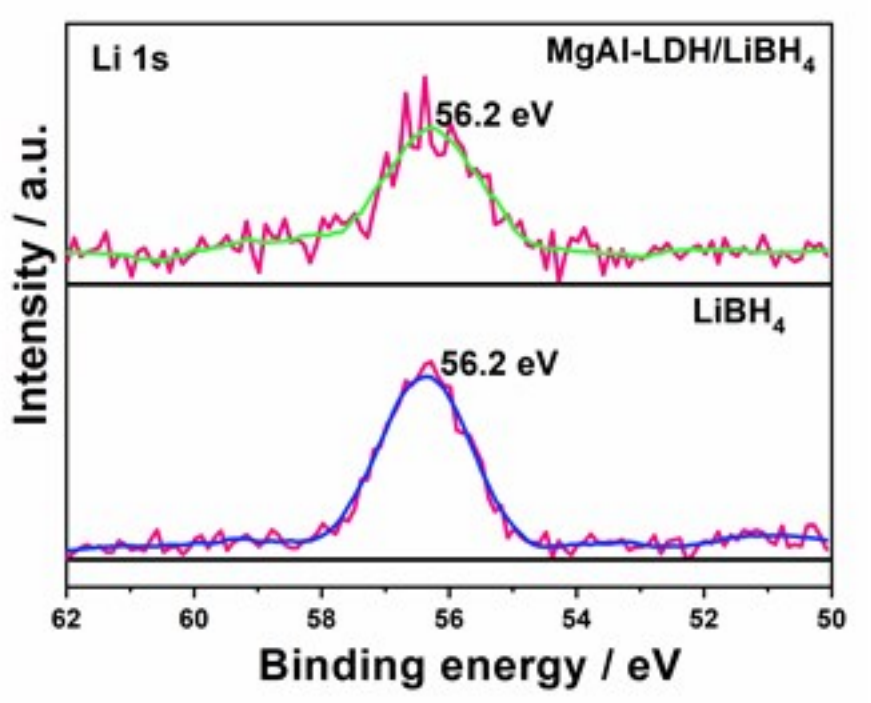

Fig. S12 The Li 1s XPS spectrum of $LiBH_4$ and MgAl-LDH/$LiBH_4$ (3:7).

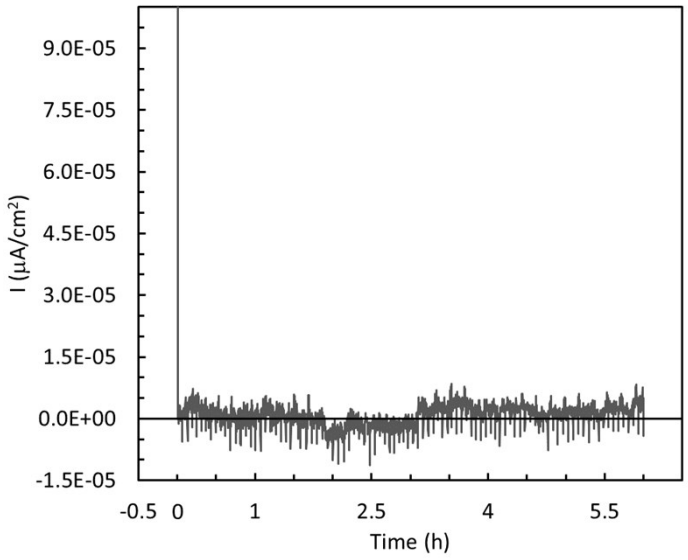

Fig. S13. The current as a function of time for MgAl-LDH/$LiBH_4$ (3:7) SSE in between two blocking stainless steel electrodes. Applied potential $\Delta V = 0.5$ V. The current decreases rapidly to zero, the plot shows the non-filtrated instrumental noise (gray line) and the mean value (black line).

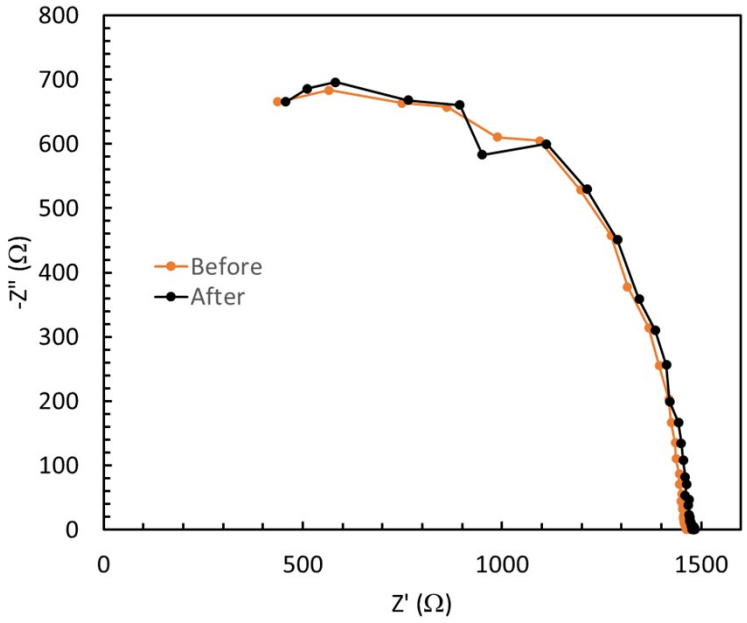

Fig. S14. Impedance spectra for MgAl-LDH/$LiBH_4$ (3:7) symmetric cell with Li electrodes before and after polarization with ΔV = 15 Mv, R^0 = 1460 Ω, R^s = 1480 Ω.

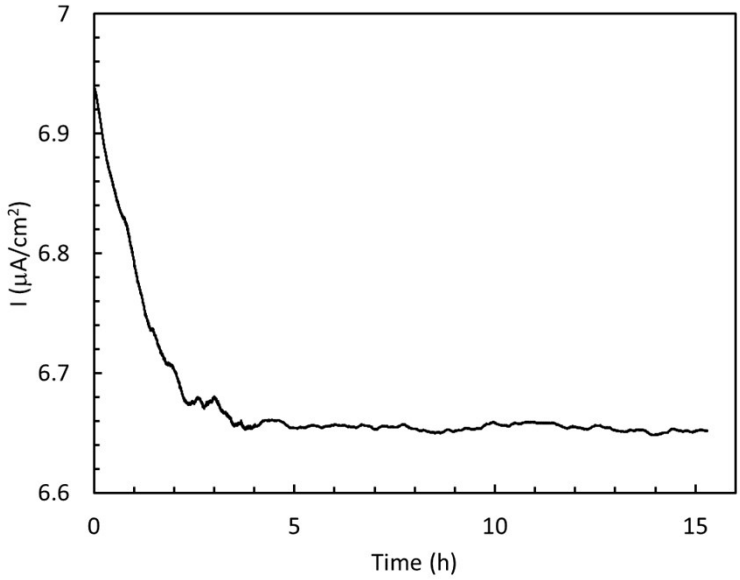

Fig. S15. Variation of current with time during polarization of MgAl-LDH/$LiBH_4$ (3:7) symmetric cell with Li electrodes (ΔV = 15 mV).

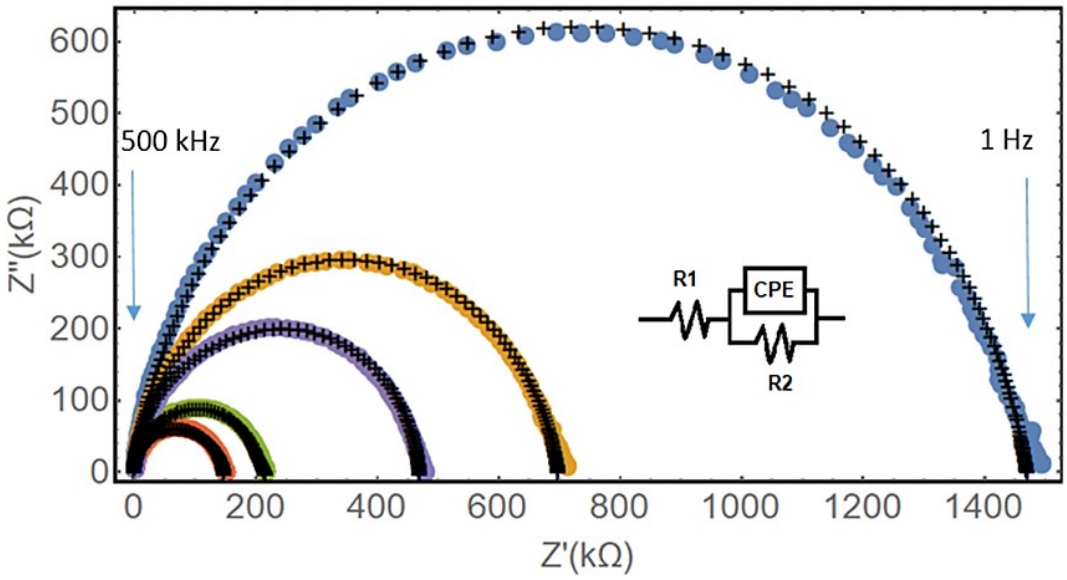

Fig. S16. Examples of the fits of the Nyquist plots for MgAl-LDH/$NaBH_4$ 7:3 using the equivalent circuit shown in insert. Blue: at 40 ºC, yellow: 60 ºC, purple: 70 ºC, green 90 ºC, red 110 ºC. The crosses are the fitted points. R1 represents any contact or wire resistance from the measuring setup, in principle negligible, while R2, intercept of the right semicircle leg with the Z' axis gives the resistivity of the SSEs.

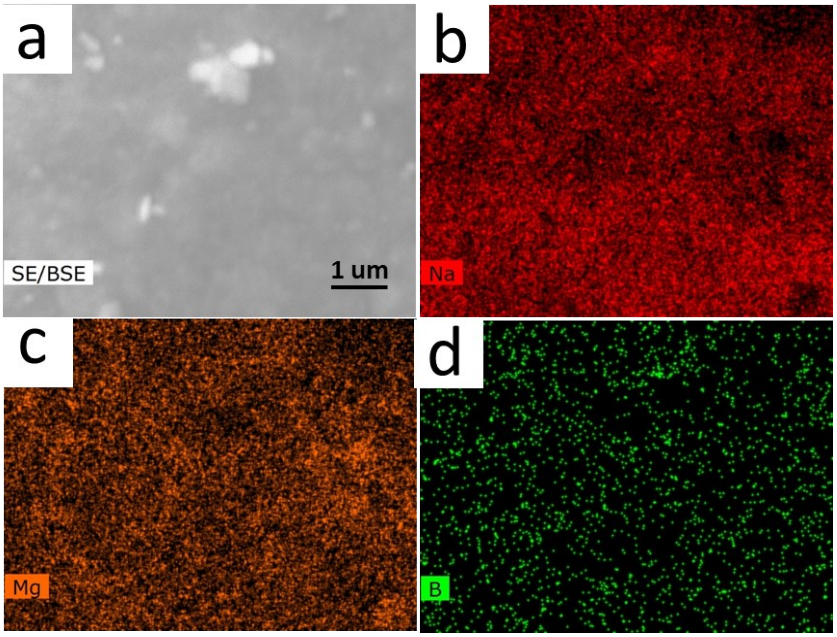

Fig. S17. SEM and EDX mapping images for MgAl-LDH/$NaBH_4$ (3:7).

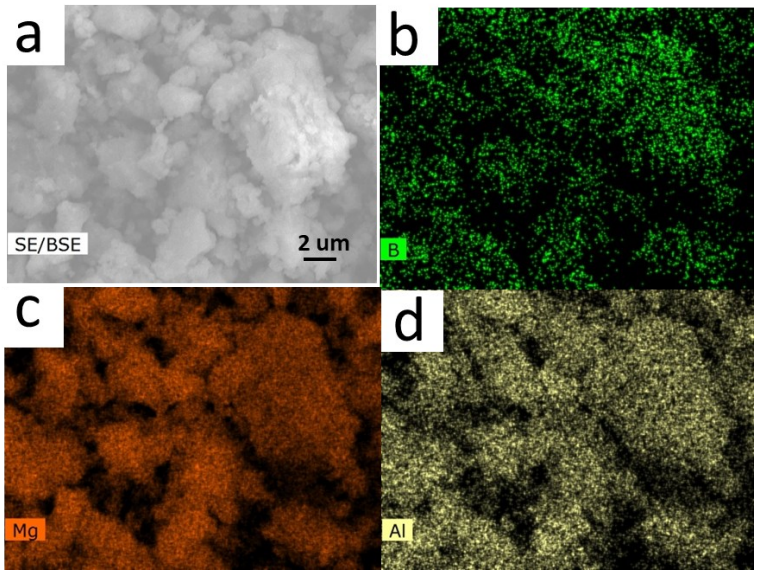

Fig. S18. SEM and EDX mapping images for MgAl-LDH/$NaBH_4$ (3:7).

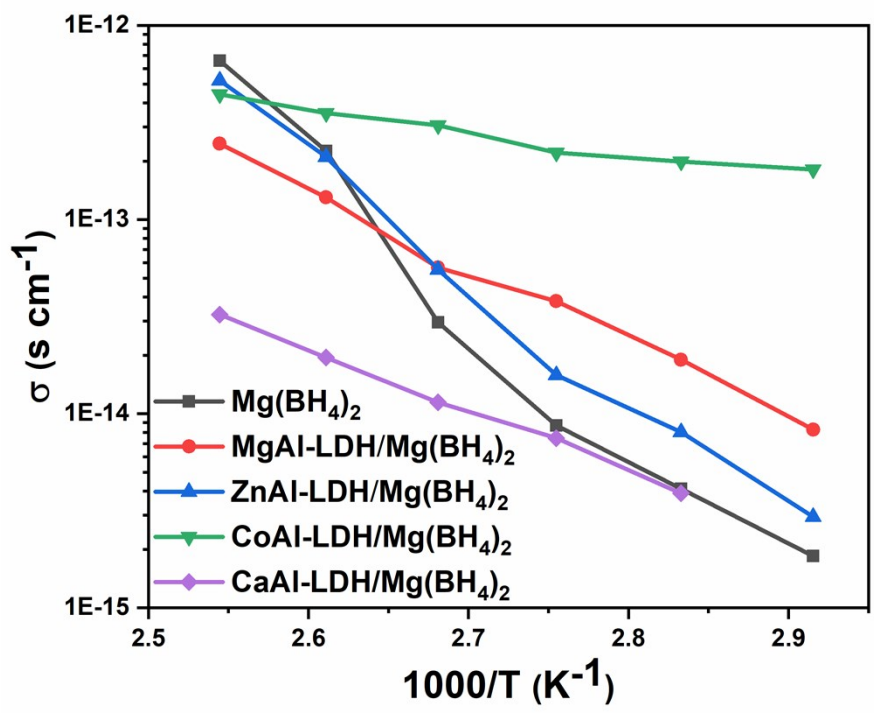

Fig. S19. Arrhenius plots of the ionic conductivities as function of temperature for various XAl-LDH/$Mg(BH_4)_2$ (3:7) SSEs.

References

[1] R. C. Agrawal, dc Polarisation: An experimental tool in the study of ionic conductors, *Indian J. pure&applied Phys.* **1999**, *37*, 294.

[2] P. G. Bruce, J. Evans, and C. A. Vincent, A dc technique for measurement of solid electrolyte conductivity, *Solid State Ionics*, **1987**, *25*, 225.

[3] J. Evans, C. A. Vincent, and P. G. Bruce, Electrochemical measurement of transference numbers in polymer electrolytes, *Polymer (Guildf)*, **1987**, *28*, 2324.

[4] P. M. Blonsky, D. F. Shriver, P. Austin, and H. R. Allcock, Complex formation and ionic conductivity of polyphosphazene solid electrolytes, *Solid State Ionics*, **1986***, 18,* 258.

[5] A. Hjorth Larsen, J. JØrgen Mortensen, J. Blomqvist, I. E. Castelli, R. Christensen, M. Dułak, J. Friis, M. N. Groves, B. Hammer, C. Hargus, E. D. Hermes, P. C. Jennings, P. Bjerre Jensen, J. Kermode, J. R. Kitchin, E. Leonhard Kolsbjerg, J. Kubal, K. Kaasbjerg, S. Lysgaard, J. Bergmann Maronsson, T. Maxson, T. Olsen, L. Pastewka, A. Peterson, C. Rostgaard, J. SchiØtz, O. Schütt, M. Strange, K. S. Thygesen, T. Vegge, L. Vilhelmsen, M. Walter, Z. Zeng, K. W. Jacobsen. The atomic simulation environment-a Python library for working with atoms. *J. Phys. Condens. Matter* **2017**, *29*, 273002.

[6] J. J. Mortensen, L. B. Hansen, K. W. Jacobsen. Real-space grid implementation of the projector augmented wave method, *Phys. Rev. B - Condens. Matter Mater. Phys.* **2005**, *71*, 1–11.

[7] J. Enkovaara, C. Rostgaard, J. J. Mortensen, J. Chen, M. Dułak, L. Ferrighi, J. Gavnholt, C. Glinsvad, V. Haikola, H. A. Hansen, H. H. Kristoffersen, M. Kuisma, A. H. Larsen, L. Lehtovaara, M. Ljungberg, O. Lopez-Acevedo, P. G. Moses, J. Ojanen, T. Olsen, V. Petzold, N. A. Romero, J. Stausholm-Møller, M. Strange, G. A. Tritsaris, M. Vanin, M. Walter, B. Hammer, H. Häkkinen, G. K. H. Madsen, R. M. Nieminen, J. K. Nørskov, M. Puska, T. T. Rantala, J. Schiøtz, K. S. Thygesen, K. W. Jacobsen. Electronic structure calculations with GPAW: a real-space implementation of the projector augmented-wave method, *J. Phys. Condens. Matter* **2010**, *22*, 253202.

[8] H. J. Monkhorst, J. D. Pack. Special points for Brillouin-zone integrations, *Phys. Rev. B* **1976**, *13*, 5188–5192.

[9] B. Hammer, L. B. Hansen, J. K. Nørskov. Improved adsorption energetics within density-functional theory using revised Perdew-Burke-Ernzerhof functionals, *Phys. Rev. B - Condens. Matter Mater. Phys.* **1999**, *59*, 7413–7421.

[10] S. Dudarev, G. Botton. Electron-energy-loss spectra and the structural stability of nickel oxide: An LSDA+U study, *Phys. Rev. B - Condens. Matter Mater. Phys.* **1998**, *57*, 1505–1509.

[11] V. Tripkovic, H. A. Hansen, T. Vegge. From 3D to 2D Co and Ni Oxyhydroxide Catalysts: Elucidation of the Active Site and Influence of Doping on the Oxygen Evolution Activity, *ACS Catal.*

2017, *7*, 8558–8571.

[12] S. Aisawa, S. Takahashi, W. Ogasawara, Y. Umetsu, E. Narita. Direct Intercalation of Amino Acids into Layered Double Hydroxides by Coprecipitation, *J. Solid State Chem.* **2001**, *162*, 52–62.

[13] Y. Filinchuk, D. Chernyshov, R. Cerny. Lightest Borohydride Probed by Synchrotron X-ray Diffraction: Experiment Calls for a New Theoretical Revision, *Jounal Phys. Chemitry C* **2008**, *112*, 10579–10584.

[14] M. D. Segall, P. J. D. Lindan, M. J. Probert, C. J. Pickard, P. J. Hasnip, S. J. Clark, M. C. Payne. First-principles simulation: ideas, illustrations and the CASTEP code, *J. Phys. Condens. Matter* **2002**, *14*, 2717–2744.

[15] M. C. Payne, M. P. Teter, D. C. Allan, T. A. Arias, J. D. Joannopoulos. Iterative minimization techniques for ab initio total-energy calculations: molecular dynamics and conjugate gradients, *Rev. Mod. Phys.* **1992**, *64*, 1045–1097.

[16] J. P. Perdew, K. Burke, M. Ernzerhof. Generalized Gradient Approximation Made Simple, *Phys. Rev. Lett.* **1996**, *77*, 3865–3868.

[17] M. Bajdich, M. García-Mota, A. Vojvodic, J. K. Nørskov, A. T. Bell. Theoretical Investigation of the Activity of Cobalt Oxides for the Electrochemical Oxidation of Water, *J. Am. Chem. Soc.* **2013**, *135*, 13521–13530.

[18] M. García-Mota, M. Bajdich, V. Viswanathan, A. Vojvodic, A. T. Bell, J. K. Nørskov. Importance of Correlation in Determining Electrocatalytic Oxygen Evolution Activity on Cobalt Oxides, *J. Phys. Chem. C* **2012**, *116*, 21077–21082.

[19] J. M. Anglada, J. M. Bofill. How good is a Broyden–Fletcher–Goldfarb–Shanno-like update Hessian formula to locate transition structures? Specific reformulation of Broyden–Fletcher–Goldfarb–Shanno for optimizing saddle points, *J. Comput. Chem.* **1998**, *19*, 349–362.